A bright monomeric near-infrared fluorescent protein with an excitation peak at 633 nm for labeling cellular protein and reporting protein-protein interaction

Feng Liu[1†], Huimin Hu[2,3†], Mengying Deng[1†], Zongqin Xiang[4†], Yuting Guo[5], Xinmeng Guan[1], Dong Li[5], Qinxue Hu[2,6], Wenliang Lei[7*], Hongjuan Peng[8*], Jun Chu[1,9*]

[1]Guangdong Provincial Key Laboratory of Biomedical Optical Imaging Technology & Center for Biomedical Optics and Molecular Imaging & CAS Key Laboratory of Health Informatics, Shenzhen Institute of Advanced Technology, Chinese Academy of Sciences, Shenzhen 518055, China

[2]State Key Laboratory of Virology, Wuhan Institute of Virology, Center for Biosafety Mega-Science, Chinese Academy of Sciences, Wuhan 430071, China

[3]Savaid Medical School, University of Chinese Academy of Sciences, Beijing 100049, China

[4]Department of Neurosurgery, the First Affiliated Hospital, Jinan University, Guangzhou, Guangdong 510630, China

[5]National Laboratory of Biomacromolecules, CAS Center for Excellence in Biomacromolecules, Institute of Biophysics, Chinese Academy of Sciences, Beijing 100101, China

[6]Institute for Infection and Immunity, St George's, University of London, London SW17 0RE, UK

[7]Guangdong-Hong Kong-Macau Institute of CNS Regeneration, Jinan University, Guangzhou, Guangdong 510630, China

[8]Department of Pathogen Biology, Guangdong Provincial Key Laboratory of Tropical Disease Research, School of Public Health, Southern Medical University, Guangzhou 510515, China

[9]Shenzhen Institute of Synthetic Biology, Shenzhen Institute of Advanced Technology, Chinese Academy of Sciences, Shenzhen 518055, China & Shenzhen-Hong Kong Institute of Brain Science

[†]These authors contributed equally

[*]Corresponding authors: leiwenliang@jnu.edu.cn or Hongjuan Peng (hongjuan@smu.edu.cn) or Jun Chu (jun.chu@siat.ac.cn)

ABSTRACT: Bright monomeric near-infrared fluorescent proteins (NIR-FPs) are useful as markers for labeling proteins and cells, and as sensors for reporting molecular

activities in living cells and organisms. However, current monomeric NIR-FPs are dim under excitation with common 633/635/640-nm lasers, limiting their broad use in cellular/subcellular level imaging. Here, we report a bright monomeric NIR-FP with maximum excitation at 633 nm, named mIFP663, engineered from *Xanthomonas campestris* pv. *Campestris* phytochrome (*Xcc*BphP). mIFP663 has high molecular brightness with a large extinction coefficient (86,600 $M^{-1}cm^{-1}$) and a decent quantum yield (19.4%), and high cellular brightness that is 3-6 times greater than those of spectrally similar NIR-FPs in HEK293T cells in the presence of exogenous BV. Moreover, we demonstrate that mIFP663 is able to label critical cellular and viral proteins without perturbing subcellular localization and virus replication, respectively. Finally, with mIFP663, we engineer improved bimolecular fluorescence complementation (BiFC) and new bioluminescent resonance energy transfer (BRET) systems to detect protein-protein interactions in living cells.

KEYWORDS: *Bacteriophytochrome, near-infrared fluorescent protein, bioluminescence resonance energy transfer (BRET), bimolecular fluorescence complementation (BiFC), protein-protein interaction*

Fluorescent proteins (FPs) with various colors have revolutionized molecular tagging and cell labeling. Of these, near-infrared FPs (NIR-FPs), whose excitation peaks are greater than 630 nm,[1-3] are particularly attractive because the long-wavelength light enables optical imaging with low photocytotoxicity and deep penetration and is spectrally compatible with GFP-like FPs and blue-green optogenetic tools. Previous studies have mainly focused on the development of red-shifted NIR-FPs (excitation peak > 670 nm) and *in vivo* applications.[2-4] However, they are not ideal for live-cell imaging *in vitro* because they exhibit low molecular brightness with quantum yields less than 9%[2] and are poorly excited by standard 633/635/640-nm red lasers in commercial microscopes. Furthermore, most of red-shifted NIR-FPs are dimeric,[4, 5] which would interfere with the function or localization of protein of interest when used as a fusion tag.

The majority of current NIR-FPs are engineered from non-fluorescent bacterial phytochromes (BphPs) and cyanobacteriophytochromes (CBCRs) that utilize endogenous biliverdin IXα (BV) in mammalian cells and exogenous phycocyanobilin (PCB) as chromophore, respectively. Specifically, monomeric NIR-FPs with excitation peaks at 630-645 nm are composed of either the PAS-GAF module of BphP (miRFP670[6] and emiRFP670[3]) or the GAF domain of CBCR (miRFP670nano[1]) with

BV covalently bound to a cysteine residue in the GAF domain. However, these NIR-FPs exhibit moderate molecular brightness and poor subcellular localization when fused to critical cellular proteins (Table 1, Figure 5). Therefore, it is highly desirable to engineer new bright monomeric NIR-FPs with improved biophysical and biochemical properties.

To address these problems, we engineered a bright monomeric NIR-FP mIFP663 from *Xanthomonas campestris* pv. *Campestris* phytochrome (*Xcc*BphP). mIFP663 is maximally excited at 633 nm and exhibits 3-6 times brighter fluorescence than other spectrally similar NIR-FPs in mammalian cells in the presence of exogenous BV. We demonstrate that mIFP663 not only is a great protein fusion tag for critical proteins but also enables the detection of protein-protein interactions (PPIs) with high sensitivity when engineered into bioluminescence resonance energy transfer (BRET) and bimolecular fluorescence complementation (BiFC) systems.

RESULTS AND DISCUSSION

Development of A Bright Monomeric NIR-FP mIFP663. An extensive literature search has revealed that the *Xcc*BphP would be a good starting point owing to three reasons. First, the PAS-GAF module (Met1-Glu320) of *Xcc*BphP shares a low amino acid sequence identity with previously reported NIR-FPs (Figure S1), raising the possibility that NIR-FPs with different biophysical properties can be engineered. Second, the crystal structure of *Xcc*BphP is available, making structure-guided directed evolution possible. Third, the PAS-GAF module of *Xcc*BphP may be naturally monomeric because it lacks strong hydrophobic interactions at the putative dimer interface, which is the case in the monomeric PAS-GAF module of *Bradyrhizobium* phytochrome (*Br*BphP) (Figure S2).

The human-codon optimized PAS-GAF module (named XFP0.1) of *Xcc*BphP (GenBank accession No. A0A0H2XCS3) was co-expressed with heme oxygenase 1 (HO-1) that produces BV in bacteria. However, the XFP0.1/BV complex was non-fluorescent. To make it fluorescent, we performed site-directed saturation mutagenesis of aspartic acid at position 199 in the DIP motif, which is crucial for 'initial fluorescence' in all BphP-based NIR-FPs.[7] As a result, a weakly fluorescent variant XFP0.2 with the D199L mutation was obtained. To blue-shift the excitation, we replaced valine at position 251 in the GAF domain with cysteine that is supposed to covalently attach to BV.[7, 8] The resultant mutant XFP0.3 was bluer by 31 nm in excitation. To improve quantum yield, we performed site-directed mutagenesis on residues near BV to reduce excited-state vibrations by tightly packing BV. Three

rounds of screening resulted in identifying a bright variant XFP0.5 with five mutations Y195F, I200T, V248M, Y255F, and S280V.

We next attempted to improve brightness by enhancing protein stability and folding. A close examination of the *Xcc*BphP structure identified several positions with destabilizing residues. Two rounds of screening led to the identification of a brighter variant XFP0.7 with five (I33V, Q93R, W102Y, M117I, and F195Y) mutations from the PAS domain and six mutations (H287R, M293L, D295A, R302K, G306A, and G309S) from the GAF domain. To optimize the folding, we screened libraries of XFP0.7 as C-terminal fusions to oligomeric Aβ42 that is known to render bright FP with poor folding weakly fluorescent.[9, 10] After 4 rounds of random mutagenesis and screening, we identified a bright fluorescent variant, dubbed mIFP663, that possesses 13 mutations: N6D, V29A, R120G, V127T, T128V, M133L, Q203L, V230M, M259I, T262S, V296L, S309G and V314E (Figure S3).

Characterization of mIFP663 *in vitro* and in Cells. mIFP663 has two absorption bands in a visible range: the Soret band at 388 nm and the Q-band at 633 nm (Figure 1a). The excitation and emission peaks are at 633 nm and 663 nm, respectively (Figure 1b and Table 1). Like miRFP670, mIFP663 behaved as a monomer at a high concentration of 10 mg/mL (Figure 1c). The peak extinction coefficient (EC) and quantum yield (QY) are 86,600 $M^{-1}cm^{-1}$ and 19.4%, respectively, resulting in a calculated molecular brightness (EC × QY) 2.5-fold and 1.6-fold brighter than miRFP670 and miRFP670nano, respectively (Table 1).

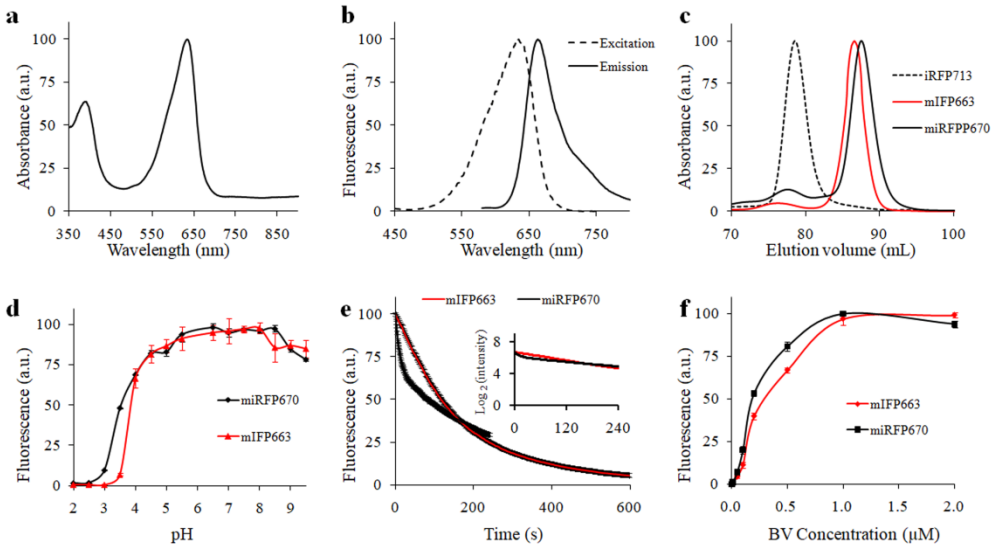

Figure 1. *In vitro* characterization of mIFP663. **(a)** Absorbance spectrum of mIFP663. **(b)** Fluorescence excitation (dashed line) and emission (solid line) spectra of mIFP663.

(c) Gel filtration of mIFP663 at a loading concentration of 10 mg/mL. miRFP670 and iRFP713 are monomer and dimer, respectively. **(d)** pH dependence of mIFP663 and miRFP670 fluorescence. **(e)** Photobleaching kinetics of mIFP663 and miRFP670 in living HeLa cells under arc lamp illumination with a 628/32-nm excitation filter. mIFP663 and miRFP670 photobleaching is single-exponential and multi-exponential fluorescence decay, respectively (insert). **(f)** BV binding to the purified mIFP663 and miRFP670. 2 μM of the apo form of mIFP663 or miRFP670 was mixed with different concentrations of free BV in PBS buffer at 37 °C, and fluorescence intensity at the emission peak was measured after 1 h incubation. All data in (d-f) are presented as mean ± standard deviation (SD) (n = 3).

Table 1 Properties of NIR-FPs with emission peak shorter than 670 nm

NIR-FP	Photoreceptor	Ex[a] (nm)	Em[b] (nm)	EC[c]	QY[d]	BR[e]	Oligomeric state	Ref.
mIFP663	*Xcc*BphP	633	663	86600[g]	19.4[g]	100	Monomer	This work
miRFP670	*Rp*BphP1	640	670	48300[g] (87400[f])	14	40 (73[f])	Monomer	6
miRFP670nano	*NpR*3784	645	670	95000[f]	10.8[f]	61	Monomer	1
emiRFP670	*Rp*BphP1	642	670	87400[f]	14[f]	73	Monomer	3
miRFP670-2	*Rp*BphP6	643	670	103000[f]	13.6[f]	83	Monomer	3
GAF-FP	*Rp*BphP1	635	670	50000[f]	7.3[f]	22	Monomer	11
iRFP670	*Rp*BphP6	643	670	114000[f]	12.2[f]	83	Dimer	12

[a]Excitation peak

[b]Emission peak

[c]Extinction coefficient ($M^{-1}cm^{-1}$)

[d]Quantum yield (%)

[e]Normalized molecular brightness (EC × QY) to that of mIFP663

[f]Values from the original papers[1, 3, 6, 9, 10]

[g]Values from this study

The fluorescence of mIFP663 was stable at a pH range of 4.5-9.0 with a pKa of 3.8 (Figure 1d). To measure the binding affinity of mIFP663 to BV, we titrated purified mIFP663 and miRFP670 apoproteins with different concentrations of free BV *in vitro*. The BV dissociation constant (K_d) for mIFP663 was approximately 2-times higher than that of miRFP670 (0.49 μM vs 0.24 μM) (Figure 1f), but lower than that of IFP1.4

(0.49 μM vs 4.2 μM).[13] mIFP663 exhibited a single-exponential fluorescence decay while the fluorescence of miRFP670 decayed multi-exponentially under arc lamp illumination (Figure 1e). Compared to miRFP670, mIFP663 is more photostable in the first 169 seconds but then less photostable.

mIFP663 was 2.9 times brighter than miRFP670 in bacteria (Figure S4a-b), which is consistent with *in vitro* result. However, the fusion protein Aβ42-mIFP663 was 8.4 times brighter than Aβ42-miRFP670 in bacteria (Figure S4a-b). Similarly, Aβ42-mIFP663 was 5 and 4.8 times brighter than Aβ42-miRFP670 in HEK293T and HeLa cells, respectively (Figure S4c-f). Taken together, these data suggest mIFP663 has higher folding efficiency than miRFP670.

We next examined cellular brightness and localization of mIFP663 in mammalian cells. The cellular brightness depends on molecular brightness, protein expression level and intracellular stability, the affinity for BV, and BV amount inside the cell.[14, 15] When expressed in HEK293T and HeLa cells, mIFP663 exhibited comparable brightness to miRFP670 without exogenous BV (Figure 2a-b), which is consistent with the fact that mIFP663 is higher in molecular brightness while the lower binding affinity for BV than miRFP670. Meanwhile, the brightness of mIFP663 and miRFP670 significantly increased after the addition of BV (Figure 2a-b), with the former being ~2.6-fold brighter under 18 h incubation with BV (Figure 2c-d). Moreover, mIFP663 was 6.2-fold and 2.1-fold brighter than miRFP670nano and emiRFP670 in the presence of exogenous BV, respectively (Figure S5). mIFP663, like miRFP670, was evenly distributed in the cytoplasm and nucleus (Figure 2a-b), indicating that it is monomeric in living cells.

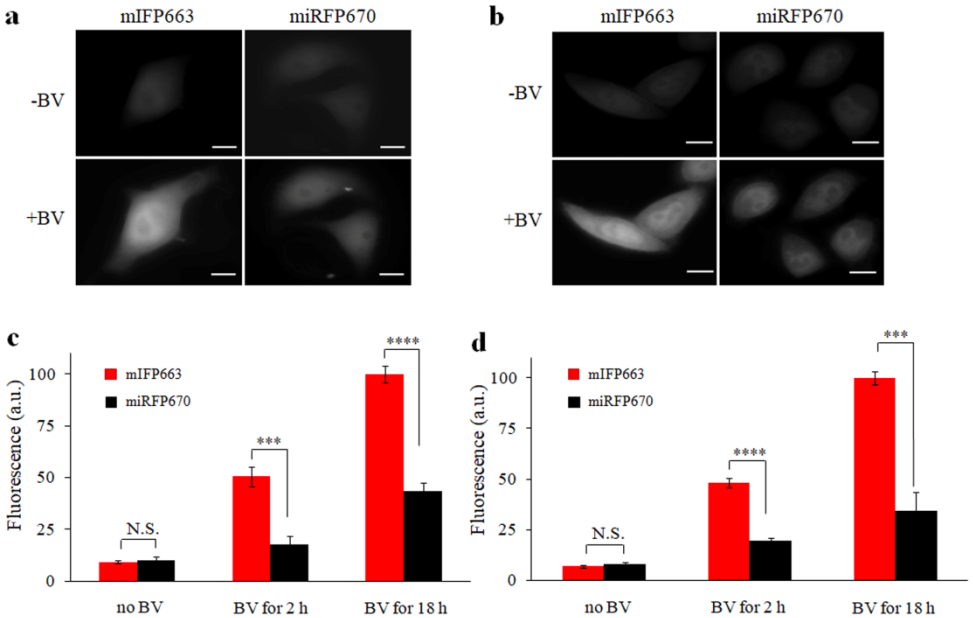

Figure 2. Brightness comparison of mIFP663 and miRFP670 in mammalian cells. **(a, b)** Representative fluorescence images of mIFP663 and miRFP670 in HEK293T (a) and HeLa (b) cells in the presence or absence of 25 μM exogenous BV. Cells expressing NIR-FP were incubated with BV and imaged at 46 h and 48 h after transfection, respectively. Scale bars, 10 μm. **(c, d)** Quantitative analysis of brightness of mIFP663 and miRFP670 in HEK293T (c) and HeLa (d) cells in the presence or absence of 25 μM exogenous BV. Cells co-expressing NIR-FP and the green FP mNeonGreen were incubated with BV at 30 h or 46 h after transfection. The fluorescence intensity was recorded on a plate reader at 48 h after transfection, respectively. All NIR fluorescence was normalized to green fluorescence from mNeonGreen. All data in (c) and (d) are presented as mean ± SD (n=3 independent experiments). Two-tailed Student's *t*-test was performed. N.S., non-significant ($P > 0.05$), ***$P < 0.001$, ****$P < 0.0001$.

We finally asked whether mIFP663 can label primary cells. mIFP663 was expressed in rat hippocampal neurons and imaged in the presence of exogenous BV. Again, whole neurons including somas, neurites (axons and dendrites) and even postsynaptic structures (dendritic spines) were filled with bright fluorescence (Figure S6), suggesting the great folding and solubility of mIFP663, which is the case for newly developed green FP mGreenlantern.[16] Taken together, mIFP663 is a good cell marker not only for cell lines but also for primary cells.

mIFP663 is an Excellent Protein Fusion Tag in Mammalian Cells. Monomeric FPs are considered to be great protein tags without perturbing subcellular localization or function of fused proteins. However, some studies have shown that monomeric or fast-folding FPs can cause severe protein mislocalization when fused to cellular proteins,[17, 18] suggesting that the monomericity or fast folding does not always correlate well with fusion performance in cells. Therefore, a systematic evaluation of different mIFP663 fusion proteins is needed.

We first examined whether mIFP663 can label subcellular targeting domains without perturbing their localizations. As expected, mIFP663-tagged proteins localized properly to common targets including actin, tubulin, plasma membrane, endoplasmic reticulum, Golgi, endosome and mitochondria (Figure 3a). In addition, the fusion of mIFP663 to histone H2B (mIFP663-H2B) did not perturb the progression of mitosis (Figure 3b). Furthermore, mIFP663-H2B, when combined with GFP-COX8A (green mitochondria) and mScarlet-I-Lifeact (red actin microfilaments), allowed 3-color imaging of three organelles in a single HeLa cell (Figure 3c).

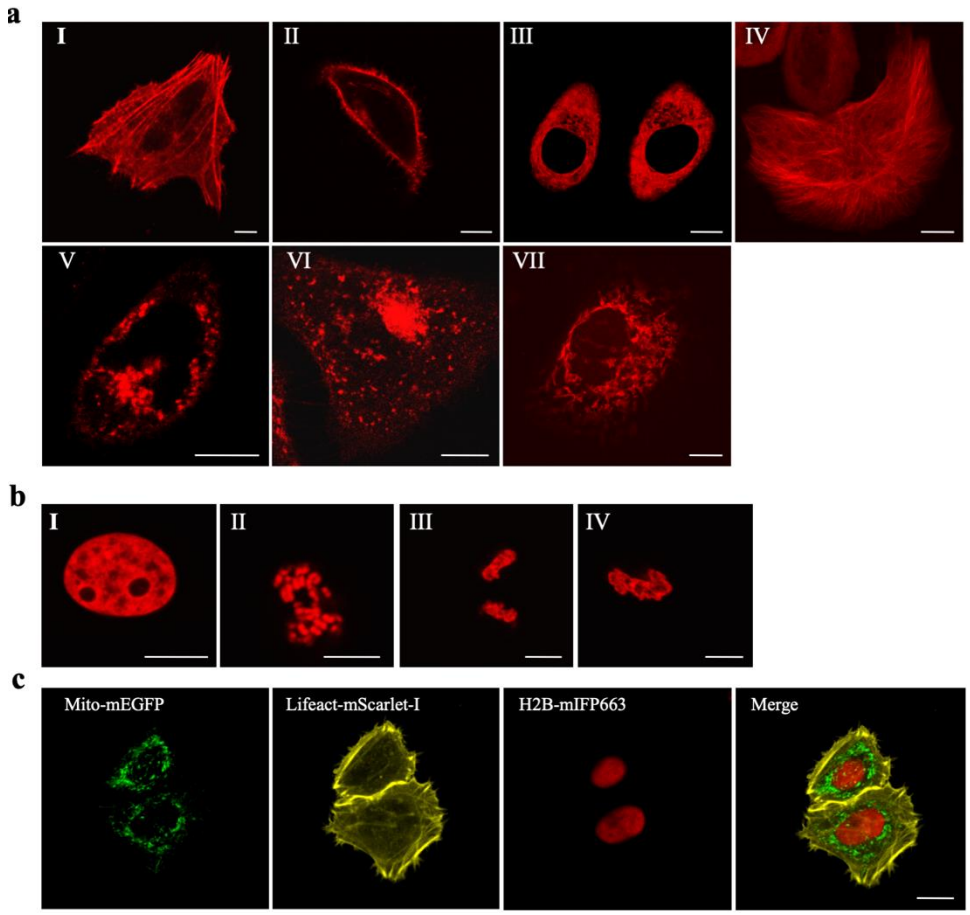

Figure 3. Confocal imaging of HeLa cells expressing mIFP663 fused to various subcellular targeting domains. **(a)** Fluorescence images of cellular organelles labelled with mIFP663. For each fusion, the linker amino acid (aa) length is indicated in between the two domains, and the origin of the fusion partner and its normal subcellular location, respectively, are indicated in parentheses: **I** mIFP663-18aa-actin (β-actin, actin cytoskeleton); **II** mIFP663-5aa-CAAX (human c-Ha-Ras 20-aa farnesylation signal, plasma membrane); **III** Calnexin-14aa-mIFP663 (human calnexin, endoplasmic reticulum); **IV** mIFP663-18aa-tubulin (human α-tubulin, microtubules); **V** B4GALT1-7aa-mIFP663 (β-1,4-galactosyltransferase 1 aa1-82, Golgi apparatus); **VI** mIFP663-14aa-RhoB (human RhoB, endosomes); **VII** COX8A-14aa-mIFP663 (human cytochrome C oxidase subunit VIIIA, mitochondria). **(b)** Fluorescence images of mIFP663-10aa-H2B (human histone 2B). **I** interphase; **II** prophase; **III** telophase; **IV** metaphase. **(c)** Three-color imaging of COX8A-$(G4S)_9$-mEGFP, Lifeact-$(G4S)_2$-mScarlet-I and mIFP663-10aa-H2B in the same HeLa cell. Transfected cells were incubated with BV and imaged at 24 h and 48 h after transfection, respectively. Scale bars, 10 μM.

Organelle-targeting fusion proteins along with super-resolution imaging techniques enable visualization of the complex dynamic of organelle with high

resolution.[19, 20] The grazing incidence structured illumination microscopy (GI-SIM) is capable of high-speed, long-term, super-resolution imaging of dynamic intracellular processes. To demonstrate the utility of mIFP663 in GI-SIM, we expressed mIFP663-COX8A in COS-7 cells and imaged them with GI-SIM microscopy.[19] mIFP663-COX8A enabled visualization of mitochondrial fine structures with high spatial resolution under 633 nm excitation (Figure 4a), suggesting that mIFP663 is bright enough for super-resolution imaging. In addition, two-color SIM imaging of GFP-tubulin and mIFP663-COX8A was achieved in the same cell (Figure 4b).

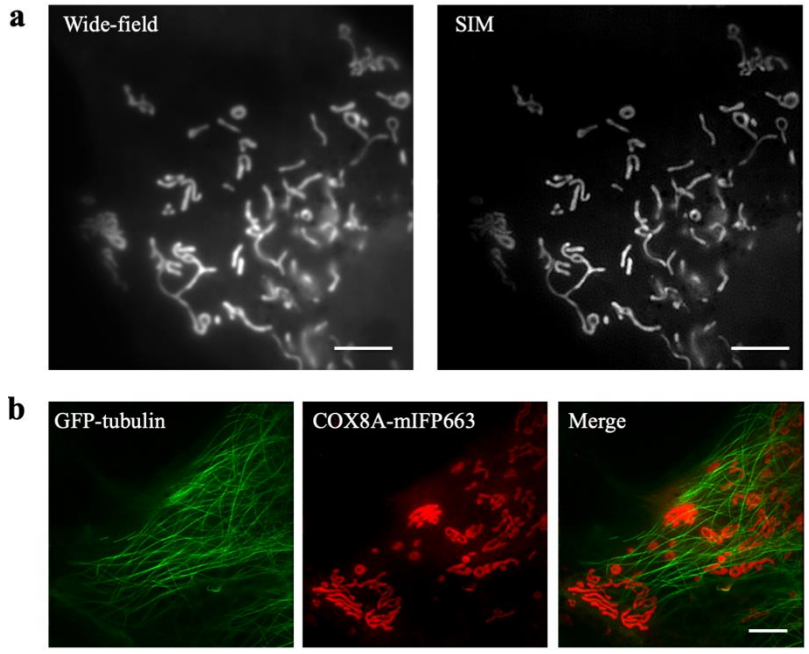

Figure 4. Wide-field and structured illumination microscopy (SIM) imaging of HeLa cells expressing FPs fused with subcellular targeting domains. **(a)** Wide-field and SIM imaging of live HeLa cells expressing COX8A-mIFP663. **(b)** Two-color SIM imaging of live HeLa cells expressing GFP-tubulin and COX8A-mIFP663. Transfected cells were incubated with BV and imaged at 24 h and 48 h after transfection, respectively. Scale bars, 5 μm.

We next explored the possibility of labeling critical proteins with mIFP663, miRFP670 and miRFP670nano. To that end, the calcium channel Orai1 and the intracellular domain of mouse Notch1 receptor (mNotch1-IC), which localize in the plasma membrane and nucleus, respectively, were used. We observed that all Orai1 fusion proteins localized correctly to the plasma membrane while mIFP663-Orai1 had less intracellular dotted structures (Figure 5), suggesting mIFP663 is more efficiently exported from Golgi and transported onto the plasma membrane. The fusion mIFP663-mNotch1-IC was evenly distributed in the nucleus in HeLa cells (Figure 5). However,

to our surprise, miRFP670-mNotch1-IC was very toxic to cells because no viable cells were found (Figure 5), and miRFP670nano-mNotch1-IC formed vesicle-like structures in the nucleus (Figure 5).

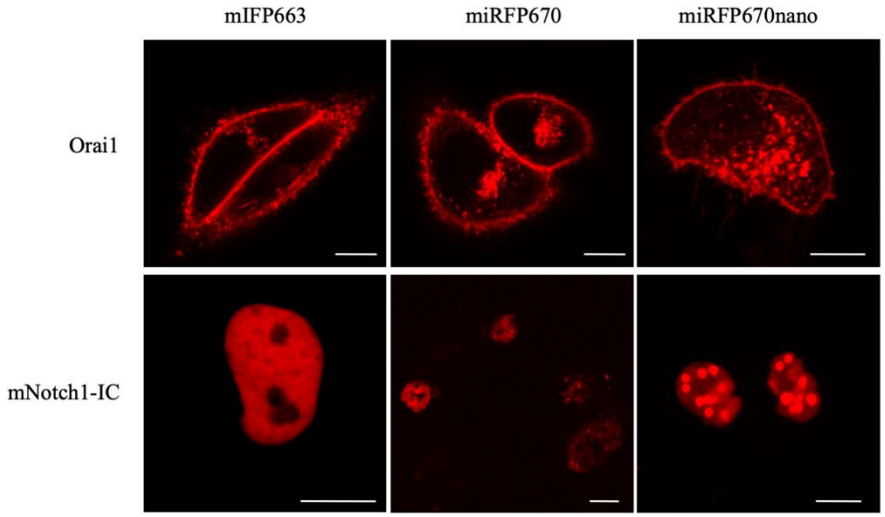

Figure 5. Confocal imaging of HeLa cells expressing mIFP663 fused to Orai1 and mNotch1-IC. Transfected cells were incubated with BV and imaged at 24 h and 48 h after transfection, respectively. Scale bars, 10 μM.

Lastly, we attempted to utilize mIFP663 as an internal tag to label cellular proteins. Some signaling proteins (e.g. Gα, α subunits of G protein) do not tolerate an FP fusion to either end, leaving only the choice of inserting FP onto highly flexible loops or disordered regions.[21, 22] A previous study has shown that the Gα13 subunit localizes on the plasma membrane without loss of biological function when internally (Arg128-Ala129) inserted with GFP.[22] Similarly, insertion of mIFP663 into Gα13 did not alter membrane localization of Gα13 (Figure S7), indicating that mIFP663 is a great protein fusion tag.[1]

mIFP663 is an Excellent Fusion Tag in HSV-2 Virion. Herpes simplex virus type 2 (HSV-2) is a prevalent human pathogen that is neurotropic and capable of establishing latent infection in host nerve ganglia.[23] It has been reported that the green FP mNeonGreen can be fused to the C-terminus of HSV-2 capsid protein VP26 (12 kD in molecular weight) to track viral infection without perturbing the virus replication efficiency.[24] However, mNeonGreen-labelled HSV-2 is not well suitable for *in vivo* imaging and is not compatible with transgenic mice expressing EGFP or EGFP-based indicators. Thus, we asked whether mIFP663 has a similar performance as mNeonGreen in labeling HSV-2 virion.

To simultaneously track virus infection and HSV-2 virion production, we constructed a dual-color labeled HSV-2 variants using the bacterial artificial chromosome (BAC). Briefly, EGFP was inserted between two unique long (UL) genes of the HSV-2 genome as previously described to indicate infected host cells,[25] while mIFP663, miRFP670, or miRFP670nano was fused to the C-terminus of VP26 to highlight HSV-2 virion (Figure 6a, Figure S8). Vero cells were transfected with BAC plasmids to produce recombinant HSV-2 variants (mIFP663 HSV-2/EGFP, miRFP670 HSV-2/EGFP, and miRFP670nano HSV-2/EGFP) and then infected with HSV-2 variants at a multiplicity of infection (MOI) of 1. As expected, green fluorescence was evenly distributed between the nucleus and cytoplasm, indicating that cells were infected by the virus, while NIR fluorescence was observed in virion clusters (red dots) (Figure 6b). However, the number of virion clusters for the mIFP663 HSV-2/EGFP variant was significantly greater than those of the other two HSV-2 variants, suggesting the great ability of mIFP663 to label viral proteins.

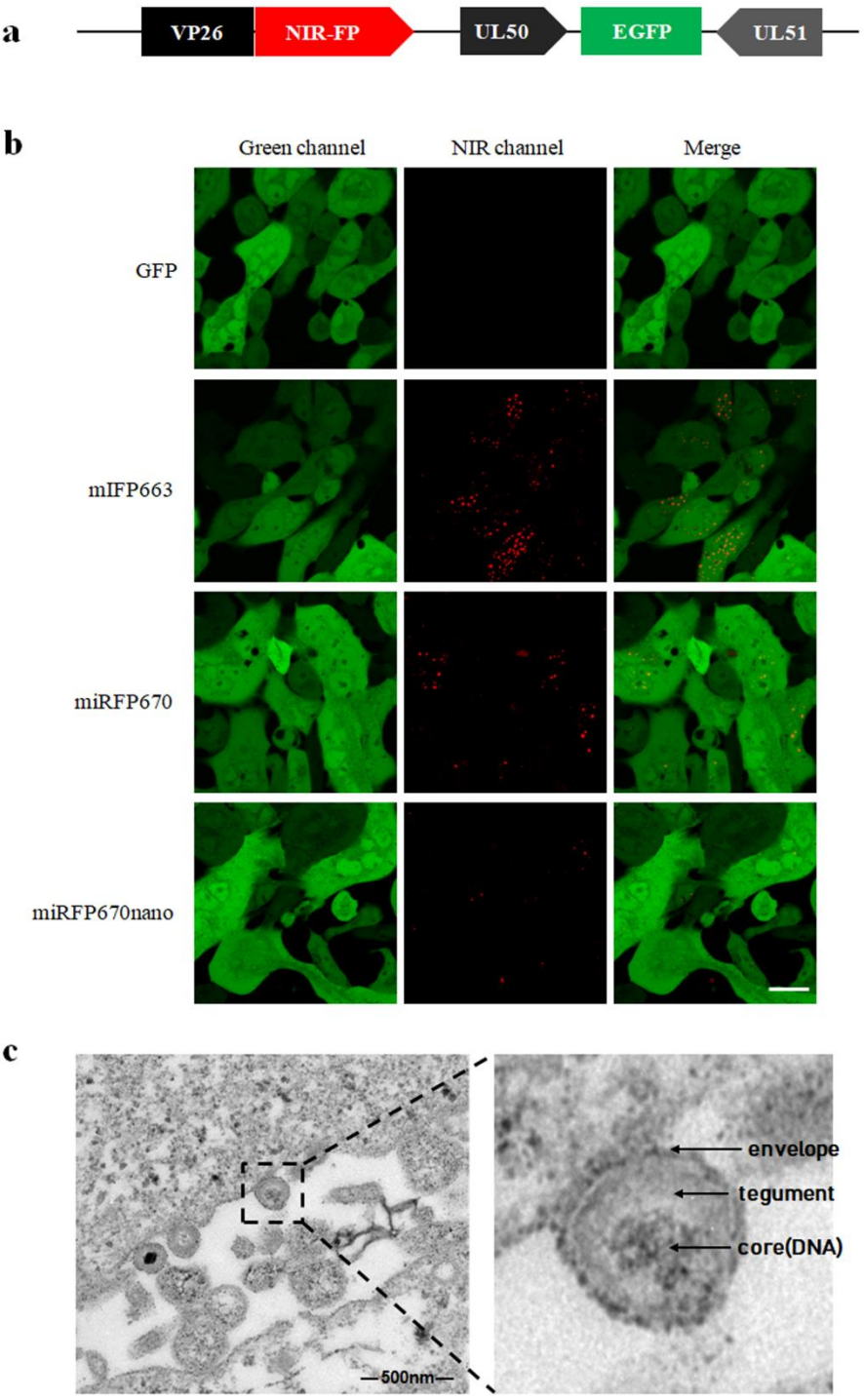

Figure 6. Performance of mIFP663 in labeling the HSV-2 virion. **(a)** Schematic diagram of the genome structure of the recombinant HSV-2 virus. **(b)** Fluorescence images of HSV-2 virus-infected Vero cells. Vero cells were infected with HSV-2/EGFP (EGFP), mIFP663 HSV-2/EGFP (mIFP663/EGFP), miRFP670 HSV-2/EGFP (miRFP670/EGFP) and miRFP670nano HSV-2/EGFP (miRFP670nano/EGFP), treated with 25 μM BV for 0.5 h at 24 h post-infection (h.p.i), and then imaged by fluorescence microscopy using a 60 × objective. Scale bars, 25 μm. **(c)** Transmission electron microscopic images of mIFP663 HSV-2 in Vero cells fixed with glutaric

dialdehyde. Black arrows from top to bottom indicate envelope, tegument, DNA core respectively, in mIFP663 HSV-2 particles. Scale bar, 500 nm.

A single intact HSV-2 virion should be spherical and consists of the nucleoprotein core, capsid shell, tegument and envelope. The core contains a linear, double-stranded DNA (dsDNA) genome, and the capsid is icosahedral and approximately 150-200 nm in diameter. Correspondingly, the electron microscopy results showed that the mIFP663 HSV-2 particle was normal in shape and size. Moreover, normal viral envelope, tegument and nucleic acid could be observed (Figure 6c), suggesting negligible cytotoxicity of mIFP663 in HSV-2 virion. Taken together, these data strongly indicate that mIFP663 is a great NIR marker for single virus tracking without compromising the virus replication efficiency.

An mIFP663-Based BiFC System for Detecting Protein-Protein Interaction in Mammalian Cells. Bimolecular fluorescence complementation (BiFC) is a technique to visualize protein-protein interactions (PPIs) in living cells, and has been widely used in various model organisms.[6, 26-29] In BiFC, a fluorescence signal is generated only when nonfluorescent fragments of FPs are brought together by interacting proteins. To date, four NIR-FPs including miRFP670 have been engineered into NIR BiFC systems.[6, 26-29] However, those BiFC systems likely have low signal-to-noise ratios because their parental NIR-FPs are dim. Given its high brightness and great folding, mIFP663 would be a good starting point to engineer an improved NIR BiFC system.

Based on structure alignments of mIFP663 and other NIR-FPs, six sites within the unstructured loop between PAS and GAF domains were selected to split mIFP663 (Figure S9a). To perform a fast screening, we fused fragments of mIFP663 to two interacting peptides K-coil and E-coil (positive control) or K-coil only (negative control), co-expressed them in bacteria, and examined fluorescence and fluorescence contrast. As a result, a NIR BiFC system with the split site between Thr127 and Val128, designated miSplit663, exhibited the highest NIR fluorescence and fluorescence contrast (Figure S9b). Notably, the reconstituted miSplit663 is ~70% dimmer than intact mIFP663, which is comparable to other NIR BiFC systems (50%-90% dimmer than their intact versions).[6, 26, 27]

We next compared the performance of miSplit663 and miRFP670-based miSplit670. FRB and FKBP proteins are engaged in the mammalian targets of rapamycin (mTOR) signaling and strongly interact with each other in the presence of rapamycin.[30] The N- and C-terminal fragments of mIFP663 or miRFP670 were fused

to the C-terminus of FKBP and FRB, respectively (Figure 7a). We expressed BiFC constructs from a tricistronic vector allowing co-expression with the green FP mNeonGreen, and used the green signal to normalize for differences in mRNA levels. We observed that, in HeLa cells, the fluorescence of miSplit663 and miSplit670 was negligible at the resting state and significantly increased after the addition of rapamycin (Figure 7b and 7c). Compared to miSplit670, miSplit663 had a 1.5-fold improvement in both fluorescence and BiFC contrast (Figure 7c), indicating that miSplit663 is an alternative and better choice for the detection of PPIs in living cells.

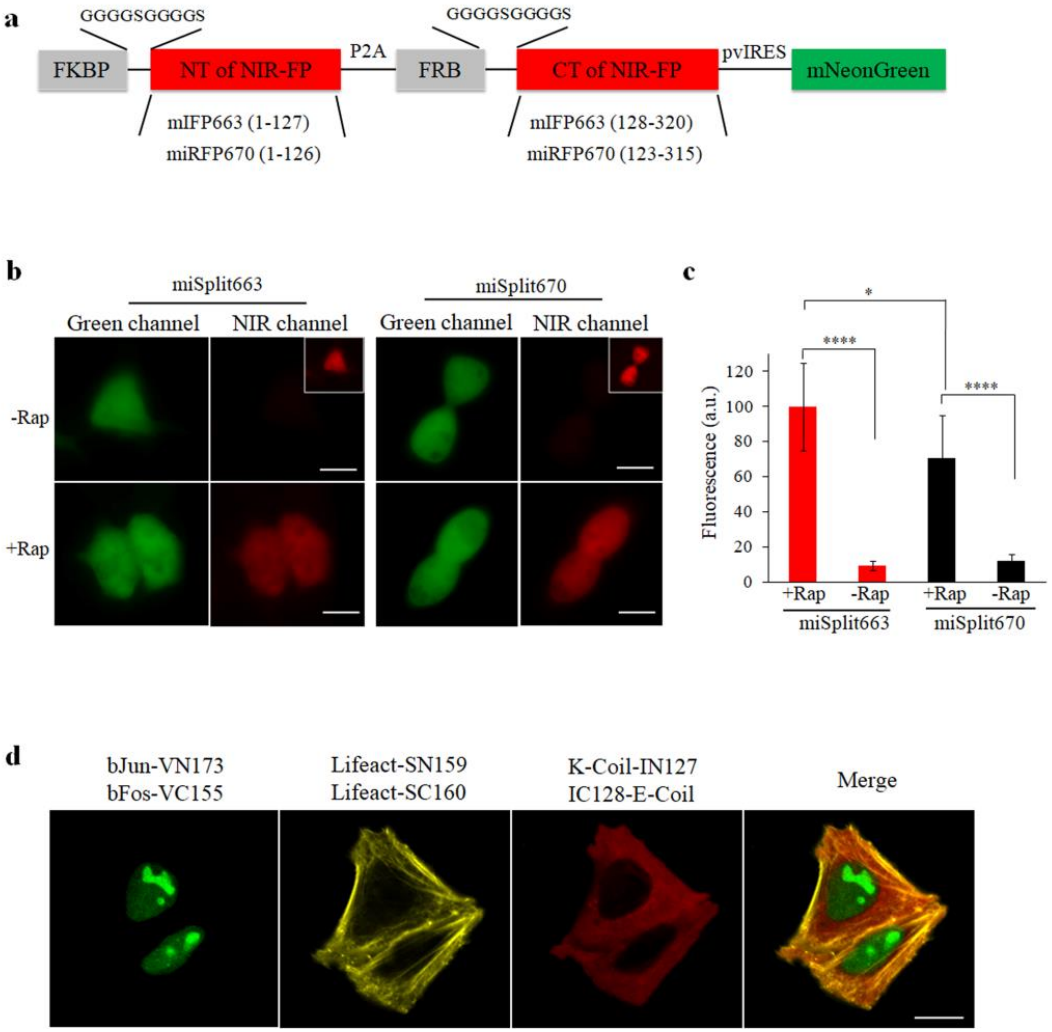

Figure 7. Visualization of protein-protein interactions with mIFP663-based NIR BiFC system in mammalian cells. **(a)** Schematics of NIR BiFC reporters for FKBP/FRB interaction. The N-terminal (NT) and C-terminal (CT) of mIFP663 or miRFP670 are fused to FKBP and FRB, respectively. P2A: 2A self-cleaving peptide from porcine teschovirus-1. pvIRES: internal ribosome entry site from poliovirus. **(b)** Fluorescence images of HEK293T cells expressing BiFC reporters. Rap is short for rapamycin. Insets with white border for the -Rap NIR channels are 10× brightened. **(c)** Fluorescence

contrast of BiFC sensors before and after the addition of rapamycin in HeLa cells. All NIR fluorescence was normalized to green fluorescence from mNeonGreen. All data are presented as mean ± SD (n=3 independent experiments). Two-tailed Student's *t*-test was performed. *$P < 0.05$，****$P < 0.0001$. **(d)** Three-color imaging of three pairs of protein-protein interactions in the same live HeLa cell with three spectrally distinct BiFC systems. The BiFC fragments of mVenus, mScarlet-I, mIFP663 are VN173/VC173, SN159/SC160 and IN127/IC128. Scale bars, 10 μM.

NIR fluorescence of miSplit663 should provide an additional color for simultaneous imaging of multiple PPIs. As a proof of concept, we fused bZIP domains of Jun and Fos (bJun and bFos) with two fragments of the yellow FP mVenus, and tagged Lifeact with two fragments of the red FP mScarlet-I. These two BiFC systems along with miSpit663 allowed to specifically visualize dimerization of bJun/bFos, Lifeact/Lifeact and K-coil/E-coil in the same live HeLa cells (Figure 7d), thus providing a means to decipher complex signaling pathways.

An mIFP663-Based BRET System for Detecting Protein-Protein Interaction in Mammalian Cells. Besides BiFC, bioluminescence resonance energy transfer (BRET) is another way to detect PPIs in mammalian cells. BRET is a transfer of energy between a bioluminescent luciferase and an FP when their distance is shorter than 10 nm.[31] Two previous studies have demonstrated that BRET can occur in the tandem fusion of dimeric NIR-FPs and the blue light-emitting luciferase Rluc owing to decent spectra overlap between the emission spectrum of Rluc and the Soret band of NIR-FP.[32, 33] However, these NIR BRET pairs are dimeric and have short Förster distances, thus not being optimal for detecting weak PPIs. To overcome these drawbacks, a BRET pair with mIFP663 and an orange-red light-emitting luciferase, in which BRET occurs via the Q band of mIFP663, is highly demanded.

The red-shifted luciferase RedFLuc with emission peak 617 nm from *Luciola Italica*[34] is a great BRET donor to mIFP663 because of significant spectral overlap between the emission spectrum of RedFluc and the Q band of mIFP663 (Figure 8b). As a demonstration, we fused FRB and FKBP to mIFP663 and RedFLuc, respectively (Figure 8a), and co-expressed them from a bicistronic vector harboring a self-cleaving viral 2A peptide. As expected, an emission shoulder around 663 nm showed up when transfected cells were treated with 100 nM of rapamycin, indicating a significant BRET signal (Figure 8c).

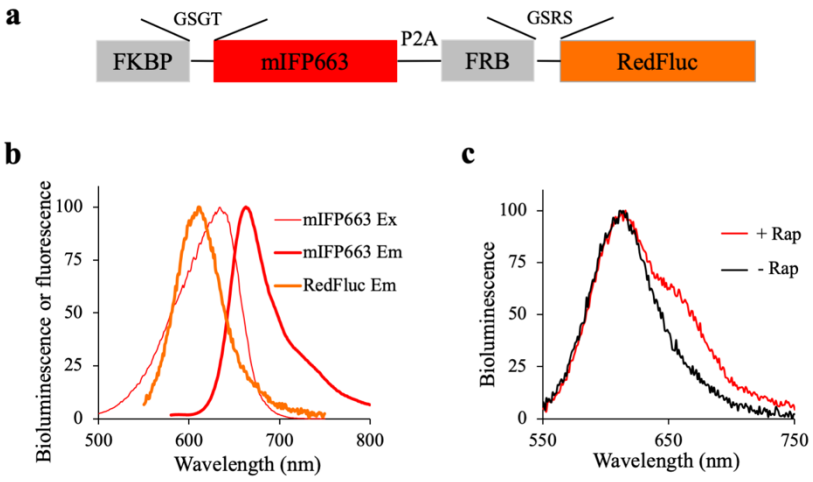

Figure 8. Detection of PPIs with mIFP663-based NIR BRET system in mammalian cells. **(a)** Schematics of NIR BRET reporter for FKBP/FRB interaction. **(b)** Bioluminescence and fluorescence spectra of RedFluc and mIFP663, respectively. **(c)** Bioluminescence spectra of NIR BRET reporter before and after the addition of rapamycin. HEK293T cells expressing NIR BRET reporter were incubated with rapamycin (final concentration of 100 nM) for 6 h prior to recording on a plate reader.

CONCLUSIONS

In this study, we describe a bright and monomeric NIR-FP mIFP663 with an excitation peak at 633 nm, engineered from the bacteriophytochrome *Xcc*BphP. To our knowledge, mIFP663 is the brightest monomeric NIR-FP in terms of molecular brightness in the presence of exogenous BV, enabling fluorescence imaging with high signal-to-background ratio. With mIFP663, cellular or viral proteins can be highlighted without the interference of subcellular location and function. Moreover, mIFP663-based BiFC and BRET systems provide powerful tools for PPI detection in living cells.

Similar to other NIR-FPs, mIFP663 requires exogenous BV to emit strong fluorescence. However, BV passes the cell membrane poorly and is easily cleared by organs *in vivo*,[5] limiting its use in deep tissue imaging. To overcome this drawback, the exogenous HO-1 can be co-expressed with NIR-FP in cells to produce a large amount of BV to generate enough fluorescent mIFP663/BV complexes.[35, 36] Alternatively, mIFP663 variants with higher binding affinity to BV could be obtained using cell-line-based screening methods in mammalian cells in the absence of exogenous BV.[37]

In conclusion, mIFP663 provides a substantial improvement over existing NIR-FPs. The applications of mIFP663 may include but are not limited to visualization of subcellular localization of proteins and PPIs at the cell level. mIFP663-based sensors could also detect protein conformation change and kinase activities, which have been realized in non-NIR sensors.[38, 39] Compared to green FPs, the potential capabilities of

mIFP663 are only beginning to be realized and will be fully explored in the future.

METHODS

Mutagenesis and Screening of Libraries. The PAS-GAF module (Met1-Glu320, Genbank accession No. A0A0H2XCS3) of *Xcc*BphP from *Xanthomonas campestris* pv.*campestris* was codon-optimized for expression in mammalian cells and synthesized by GenScript (Nanjing, China). Site-directed mutagenesis was performed by overlap-extension PCR using PrimeSTAR Max DNA Polymerase (Takara). All PCR products were ligated into a constitutive bacterial double expression vector pJC using In-Fusion HD enzyme (Takara). In the pJC vector, the expression of NIR-FP and *Synechocystis* HO-1 were driven by T7 and EM7 promoters, respectively. The Stellar competent cells (Clontech) were used for cloning and protein expression. Libraries of mutants including NIR-FP and Aβ42-NIR-FP fusion were incubated overnight at 34 ℃ on LB agar plate and maintained thereafter at room temperature. Fluorescence was imaged on plates. Colonies expressing mutants were screened for fluorescence in a dark enclosure with a white Mi-LED fiber-optic light source (Edmund, USA), 610/13-nm excitation and 687/75-nm emission filters (THORLABS), and an MDK 41 BU02 CCD camera controlled with Micro-Manager 1.4.21 (NIH). Bacterial colonies of interest were patched on LB agar plates and incubated overnight at 34 ℃. The brightest FP in each round was chosen for the subsequent round of mutagenesis.

Protein Expression in Bacteria and Characterization *in vitro*. cDNAs of NIR-FPs were cloned into the pJC vector with a polyhistidine tag on the N terminus and expressed in Stellar cells. Proteins were purified using cobalt-chelating affinity chromatography (Pierce), eluted with PBS containing 100 mM imidazole, and desalted using Econo-Pac 10 DG desalting columns (Bio-Rad).

Excitation, emission and absorbance spectra of recombinant proteins were measured with the Infinite M1000 PRO microplate reader (Tecan). For determination of extinction coefficient, a ratio of maximum absorbance values of Q and Soret bands was calculated, assuming the latter to have extinction coefficient of the free BV, which is 39900 $M^{-1}cm^{-1}$. Quantum yields were determined by integration of emission curves corrected for detector sensitivity, using miRFP670 as a standard (quantum yield 0.14). pH titrations were performed using a series of buffers (1 M HOAc, 1 M NaOAc, 5 M NaCl for pH 3.0-4.5; 1 M NaH_2PO_4, 1 M Na_2HPO_4, 5 M NaCl for pH 5.0-9.0; 100 mM glycine for pH 9.5 and 10). 5 μL of purified protein was diluted in 195 μL buffer with different pH values, and the fluorescence intensity was measured.

To perform size exclusion liquid chromatography, 200 μL volumes of the purified mIFP663, miRFP670 or iRFP713 samples were applied on the Superdex 2000 Increase

10/300 GL column (GE Healthcare) equilibrated with PBS buffer pH 7.0. A 1 mL min^{-1} flow rate was used. The concentration of proteins is 10 mg mL^{-1}.

Cell Culture and Transfection. Human HEK293T, HeLa, and Vero cells were grown in a DMEM medium (Hyclone) supplemented with 10% fetal bovine serum (Hyclone) and 1% penicillin-streptomycin (Thermo Fisher Scientific). For transient transfection with a plasmid, HEK293T or HeLa cells were transfected in a 24-well cell culture plate (Corning) using Lipofectamine 2000 (Invitrogen) following the manufacturer's protocol.

Brightness Comparison of NIR-FPs in Mammalian Cells. DNA fragmen ts mNeonGreen-P2A-mIFP663, mNeonGreen-P2A-miRFP670 and mNeonGreen-P 2A-miRFP670nano, were PCR amplified using PrimeSTAR Max DNA Polymer ase (Takara) with primers containing 5' *Kpn*I and 3' *Eco*RI restriction enzyme sites. PCR fragments were gel purified (OMEGA Gel Extraction Kit) and were ligated into a *Kpn*I/*Eco*RI double digested pcDNA3.1 vector using In-Fusion HD enzyme to make pC3.1-mNeonGreen-P2A-NIR-FP constructs.

For fluorescence measurement, HEK293T or HeLa cells were transfected with pC3.1-mNeonGreen-P2A-NIR-FP constructs, transferred into 96-well plates after 24 h transfection, and then cultured for another 24 h before recording. BV molecule (5 mM in DMSO) was added to growth media with a final concentration of 25 μM at 2 h and 18 h prior to measurement. The fluorescence intensity was recorded on the Infinite M1000 PRO microplate reader (Tecan) with the excitation and emission wavelength at 630/20 nm and 675/20 nm, respectively.

For fluorescence imaging, HEK293T or HeLa cells were transfected with pC3.1-mNeonGreen-P2A-NIR-FP constructs, transferred into 20 mm glass-bottom dishes (In Vitro Scientific) after 24 h transfection, and then cultured for another 24 h before imaging. Transfected cells were incubated with 25 μM BV molecule for 24 h prior to imaging. Transfected cells were washed twice with 1 mL imaging solution (Invitrogen), and imaged in 2 mL imaging solution. Fluorescence imaging was performed on Olympus IX83 inverted microscope with a 40 × 1.2 numerical aperture (NA) oil immersion objective lens. The excitation and emission filters are 628/32 nm and 649 nm long pass, respectively.

Confocal imaging of mIFP66 in neurons. All coverslips for hippocampal neuron cultures were coated with 0.1 mg/mL poly-d-lysine 24 h before dissection. Hippocampi from E18.5 rat embryos were digested with 0.25% trypsin for 15 min at 37 °C, followed by trituration with pipettes in the plating medium (DMEM with 10% FBS and 10% F12). After culturing for 24 h, media were changed into neuronal culture media (neurobasal media containing 1% glutamate and 2% B27).

Dissociated neurons were transfected by Lipofectamine 2000 Reagent (ThermoFisher Scientific) according to the manufacture's instruction. Transfected neurons were incubated with 25 uM of BV for 12 h and imaged at 48 h after transfection. Immediately before imaging, neurons were changed from the culture medium to the imaging medium (140 mM NaCl, 5 mM KCl, 2 mM $CaCl_2$, 1.5 mM $MgCl_2$, 10 mM glucose, and 25 mM Hepes, pH 7.4), and were warmed to 37 °C in a heating chamber. Live images were taken using a confocal microscope (Carl Zeiss LSM 700) with an oil 63× objective (NA = 1.4, Plan-Apo) and a 633 nm laser. The same acquisition settings (laser power, pinhole size, gain, etc.) were applied to all cells.

Fusion Gene Construction and Fluorescence Imaging. For the creation of mIFP663 fusion proteins, the cDNA of mIFP663 was PCR amplified with a 5' primer encoding an *Age*I site and 3' primer encoding either a *Bgl*II (C1) or *Not*I (N1) site, and the PCR products were purified (OMEGA Gel Extraction Kit) and ligated into similarly digested pEGFP-C1 or pEGFP-N1 vector backbones using In-Fusion HD enzyme. The resulting plasmids were named pmIFP663-N1 and pmIFP663-C1. In order to construct plasmids encoding mIFP663 fusions, fragments encoding various protein domains were excised from existing plasmids encoding mEmerald fusions using available restriction sites and ligated into similarly digested pmIFP663-N1 and pmIFP663-C1 vector backbones. Domains or fusion proteins were derived from the following sources: human β-actin, P60709; c-Ha-Ras, NM_001130442.1; human Golgi, NM_173216.2; human calnexin, NM_001024649; human RhoB, NM_004040.2; human H2B, NM_021058.3. To label mNotch1-IC (Mus musculus, BAC77038.1) and Orail1 (Homo sapiens, NM_032790.3) with mIFP663, miRFP670 and miRFP670nano, DNA fragments of mNotch1-IC-mIFP663, mNotch1-IC-miRFP670, mNotch1-IC-miRFP670nano, mIFP663-Orail1, miRFP670-Orail1 and miRFP670nano-Orail1 were PCR amplified and ligated into pcDNA3.1 vector using *Kpn*I and *Eco*RI. HeLa cells were grown and transfected with constructs as mentioned above. For the creation of fusion proteins for three-color imaging, the DNA fragments of COX8A-mEGFP, Lifeact-mScarlet-I and H2B-mIFP663 were amplified and inserted into pcDNA3.1 using *Kpn*I and *Eco*RI sites.

For confocal imaging, HeLa cells were transfected with fusion gene constructs, transferred into 20-mm glass-bottom dishes (In Vitro Scientific) after 24 h transfection, and then cultured for another 24 h before imaging. Transfected cells were incubated with 25 μM BV molecule for 24 h prior to imaging, washed twice with 1 mL imaging solution (Invitrogen), and imaged in 2 mL imaging solution. Fluorescence imaging was performed on Leica TCS SP5 confocal microscope with a 63 × 1.4 NA oil immersion

objective. The excitation laser and emission filters are 633 nm and 650-730 nm.

For grazing incidence structured illumination microscopy (GI-SIM) imaging , COS-7 cells were grown in DMEM media (GIBCO) supplemented with 10% fetal bovine serum (GIBCO) and 1% penicillin/streptomycin at 37°C and 5% CO_2 until 60% to 80% confluency was reached. 35 mm coverslips were pre-coated with 50 mg/mL collagen for 1 hour, and cells were then seeded onto the coverslips to achieve ~70% confluence prior to transfection. Transfections were executed using Lipofectamine 3000 (Invitrogen) according to the manufacturer's protocol. Cells were imaged 16-36 hours post-transfection in a microscope stage top micro-incubator (OKO Lab) maintained at 37°C and 5% CO_2. GI-SIM system at the Institute of Biophysics, Chinese Academy of Sciences was previously described.[19] All images were acquired with the Olympus 1.7-NA objective under the physiological conditions of 37°C and 5% CO_2.

Photobleaching of NIR-FP in Mammalian Cells. To determine photostability, HeLa cells were transfected with pmIFP663-10aa-H2B and pmiRFP670-10aa-H2B constructs. BV molecule was added to growth media with a final concentration of 25 μM at 24 h before imaging. Photobleaching was performed on Olympus IX83 inverted microscope with a 40 × 1.2 NA oil immersion objective. Fluorescence intensity was corrected to absorbance spectra, extinction coefficient, the power spectrum of 3.45 mW metal halide lamp and the transmission of emission filter (649 LP nm).

Engineering of mIFP663-based BiFC System. The mIFP663 protein was split at six positions: 124/125, 127/128, 128/129, 130/131, 131/132 and 119/122 (the tetrapeptide 119Pro-120Gly-121Asp-122Ala are present in both fragments). To screen the best split position in bacteria, the PAS or GAF domain in the 'pWa PAS-E BAD K-GAFm' plasmid (Addgene no. 39866) was replaced by corresponding split fragments of mIFP663. The negative control plasmids were constructed by removing the E-coil fragment. All split plasmids were expressed in *E. coli*, and proteins were induced when OD_{600} reached 0.4-0.6 using 0.02% arabinose and 0.2% rhamnose. After 24 h induction, the fluorescent intensity of *E. coli* cells was measured using the Infinite M1000 PRO microplate reader (Tecan). The fluorescence intensity was normalized to OD_{600}.

BiFC Imaging of Protein-Protein Interaction. The fragments of FKBP-CT, NIR-FP-P2A-FRB-NT, and NIR-FP-pvIRES-mNeonGreen were generated by overlap PCR using primers containing *Bam*HI and *Eco*RI and was ligated into a similarly digested pcDNA3.1 vector using In-Fusion HD enzyme.

To determine the complementation contrast in mammalian cells, HEK293T cells were transfected, transferred into 20-mm glass-bottom dishes (In Vitro Scientific) after 24 h transfection, and then transferred from 6-well plate into 96-well plate. BV and

rapamycin were added to growth media with a final concentration of 25 μM and 100 nM, respectively, and were incubated for 24 h prior to measurement. The fluorescence intensity was recorded on the Infinite M1000 PRO microplate reader (Tecan) with the excitation and emission wavelengths at 630/20 nm and 675/20 nm, respectively.

For fluorescence imaging, HEK293T cells were transfected with miSplit663 and miSplit670 reporter plasmids and transferred onto 20-mm glass-bottom dishes (In Vitro Scientific) after 12 h transfection. After 24 h transfection, BV and rapamycin were added to the culture medium at final concentrations of 25 μM and 100 nM, respectively. Fluorescence cells were changed culture medium with imaging buffer and then imaged at 48 h post-transfection. Fluorescence imaging was performed on Olympus IX83 inverted microscope with a 40 × 1.2 NA oil immersion objective. The excitation and emission filters are 628/32 nm and 649 LP nm, respectively.

For three-color BiFC imaging, BiFC reporters of mVenus, mScarlet-I, mIFP663 were constructed as follows: the fragments of bJun-$(G4S)_2$-mVenus-C173-P2AT2A-bFos-$(G4S)_2$-mVenus-N155, Lifeact-$(G4S)_2$-mScarlet-I-N159-P2AT2A-Lifeact-$(G4S)_2$-mScarlet-I-C160 and K-Coil-GGS-mIFP663-N127-P2AT2A-mIFP663-C128-GGSAS-E-Coil were amplified and inserted into pcDNA3.1 using *Kpn*I and *Eco*RI sites. HeLa cells were co-transfected with BiFC reporters at a ratio of 1:1:1:1, transferred onto 20-mm glass-bottom dishes (In Vitro Scientific) after 24 h transfection, and then cultured for another 24 h before imaging. Transfected cells were incubated with 25 μM BV molecule for 24 h prior to imaging, washed twice with 1 mL imaging solution (Invitrogen), and imaged in 2 mL imaging solution. Fluorescence imaging was performed on Leica TCS SP5 confocal microscope with a 63 × 1.4 NA oil immersion objective. The excitation laser and emission filters are 633 nm and 650-730 nm, respectively.

BRET Detection of Protein-Protein Interaction. FKBP and FRB were amplified from CFP-FRB (MA) and Lyn-FKBP plasmids provided by Dr. Michael Z. Lin at Stanford University. The fragment of FKBP12-GSGT-mIFP663-P2A-FRP-GSRS-RedFluc was generated by overlap PCR using primers containing *Bam*HI and *Eco*RI and was ligated into a similarly digested pcDNA3.1 vector using In-Fusion HD enzyme.

HEK293T cells were transfected with the above BRET plasmid using Lipofectamine 2000 (Invitrogen) following the manufacturer's protocol. Cells were transferred from 6-well cell plate to 96-well plate after 24 h transfection and cultured for another 24 h. 25 μM BV and 100 nM rapamycin were added at 12 h and 24 h prior to bioluminescence detection, respectively. Bioluminescence spectrum was recorded on the Infinite M1000 PRO microplate reader (Tecan).

Virus Propagation. Wild-type HSV-2/EGFP, carrying the complete genome of HSV-2 with EGFP tag was kindly provided by Dr. Yasushi Kawaguchi (University of Tokyo, Tokyo, Japan). The virus was grown and titered on Vero cells. The virus stock was stored at − 80 °C before use infection.

Construction of NIR-FP HSV-2 Variants and Fluorescence Imaging. The *E.coli* strain DY380 containing λ-Red recombination system was kindly provided by Dr. Minhua Luo (Wuhan Institute of Virology, Chinese Academy of Sciences, Wuhan, China) and served as the parental strain for construction of NIR-FP HSV-2/EGFP BAC plasmids. Overlap PCR was used to obtain the fragments containing the NIR-FP gene, *kanamycin* (Kan) resistance gene and 50 bp upstream and 50 bp downstream extension homologous to HSV-2 UL35 gene. The overlapping primers used were as follows: Kan (Forward: TCAGAAGAACTCGTCAAGA, Reverse: GGGGGAAAGGGGGGCAACGAGAGACGGCCGCGGAGGGACCCGCCGAGGACGTTCAGGTGGCACTTTTCGG); HSV-2 UL35 upstream and downstream region (Forward: TTTGGGGGTGGAGCGGAC, Reverse: GCTGGTGGTGGTTTCCACG), miRFP670 (Forward: GCACGTATTCCCCCTTTGTCGTTCGCGACCCCAAGACCCCCAGCACCCCGAACTCGAGCGTAGCAGGTCATGCCTCT, Reverse: TCTTGACGAGTTCTTCTGATCAGCTCTCAAGCGCGGT), miRFP670nano (Forward: GCACGTATTCCCCCTTTGTCGTTCGCGACCCCAAGACCCCCAGCACCCCGAACTCGAGCGCAAACCTGGACAAGATG, Reverse: TCTTGACGAGTTCTTCTGATCAGCTCTGCTGGATGGC). mIFP663 (Forward: GCACGTATTCCCCCTTTGTCGTTCGCGACCCCAAGACCCCCAGCACCCCGAACTCGAGCGTGAGCACCGCTACCGAT, Reverse: TCTTGACGAGTTCTTCTGATCACTCCAGCCTGGCTCT). 5 mg purified PCR products were electroporated into 50 μL of competent DY380 cells containing HSV-2/EGFP BAC, with the settings of 1.8 kv, 25 mF, and 200 V. 1 mL LB medium was added and the transformed cells were then incubated at 32˚C for 2 h with shaking. Subsequently, 100 μL cultures were plated onto an agar plate containing 50 mg/mL kanamycin (Kan) and 34 mg/mL chloramphenicol (Cam). NIR-FP HSV-2/EGFP variants were confirmed by PCR detection and DNA sequencing. The NIR-FP HSV-2/EGFP BAC was extracted using Plasmid DNA purification kit (NucleoBond XtraMidi/Maxi). The NIR-FP HSV-2 BAC plasmid was then transfected into Vero cells using Lipofectamine 3000 (Invitrogen) following the manufacturer's protocol to produce viruses.

Vero cells were seeded in 35-mm glass-bottom dishes and infected with wild-type HSV-2 or NIR-FP HSV-2 variants. At 24 h post-infection, cells were treated with 25 μM BV for 0.5 h, and then fixed with 4% paraformaldehyde at room temperature for

10 min. After washes, cells were imaged under a fluorescence microscope (Nikon A1R/MP). The excitation laser and emission filters are 640 nm and 663-738 nm, respectively.

Transmission Electron Microscopy. Vero cells were seeded in 10-cm dishes and infected with mIFP663 HSV-2. At 24 h post-infection, cells were treated with glutaric dialdehyde and fixed overnight before collected for electron microscopy. After sectioning and staining, the virus particles were observed under a 200 kV transmission electron microscope.

Statistics. The statistical significances between groups were determined using two-tailed Student's *t*-tests in Excel. N.S., non-significant ($P > 0.05$), $*P < 0.05$, $**P < 0.01$, $***P < 0.001$, $****P < 0.0001$.

Supporting Information Available: The following files are available free of charge.
Figure S1. Sequence alignment of NIR-FPs and the PAS-GAF module of *Xcc*BphP; Figure S2. Rational design of mIFP663; Figure S3. Sequence alignment of best XFP variants from each round of screening; Figure S4. Brightness comparison of mIFP663 and miRFP670 fused to the Aβ42 peptide in *E.coli* and mammalian cells; Figure S5. Brightness comparison of mIFP663, miRFP670nano and emiRFP670 in mammalian cells; Figure S6. Confocal imaging of E18.5 dissociated rat hippocampal neurons expressing mIFP663; Figure S7. Confocal imaging of Hela cells expressing mIFP663-Gα13; Figure S8. Flow chart of the generation of NIR-FP HSV-2/EGFP viruses; Figure S9. Brightness of different reconstituted split mIFP663 fragments that are fused with interacting K-Coil and E-Coil peptides.

Author Contributions

J.C. conceived and supervised the study. F.L., H.H., H.P., D.L. and J.C. designed the study. F.L. performed protein engineering of mIFP663, *in vitro* characterization, and imaging of fusion proteins and PPIs. H.H. performed HSV-2 experiments. M.D. performed experiments in HEK293T/HeLa cells and bacteria. Z.X. and W.L. performed mIFP663 imaging in neurons. T.G. performed GI-SIM imaging; F.L., H.H., X.G., and J.C. wrote the manuscript with input from other authors.

ACKNOWLEDGMENTS

This work was supported by National Key Research and Development Program of China (2017YFA0700403, 2020YFA0908802, 2021YFF0502904), National Natural Science Foundation of China (81927803, 21874145, 32000732, 32000731), Guangdong Basic and Applied Basic Research Foundation (2020B121201010,

2020A1515010675), Natural Science Foundation of Shenzhen (JCYJ20200109115633343).

Notes

The authors declare no competing financial interest.

REFERENCES

(1) Oliinyk, O. S.; Shemetov, A. A.; Pletnev, S.; Shcherbakova, D. M.; Verkhusha, V. V. Smallest Near-Infrared Fluorescent Protein Evolved from Cyanobacteriochrome as Versatile Tag for Spectral Multiplexing. *Nat. Commun.* **2019,** *10* (1), No. 279.

(2) Piatkevich, K. D.; Suk, H. J.; Kodandaramaiah, S. B.; Yoshida, F.; DeGennaro, E. M.; Drobizhev, M.; Hughes, T. E.; Desimone, R.; Boyden, E. S.; Verkhusha, V. V. Near-Infrared Fluorescent Proteins Engineered from Bacterial Phytochromes in Neuroimaging. *Biophys. J.* **2017,** *113* (10), 2299-2309.

(3) Matlashov, M. E.; Shcherbakova, D. M.; Alvelid, J.; Baloban, M.; Pennacchietti, F.; Shemetov, A. A.; Testa, I.; Verkhusha, V. V. A Set of Monomeric Near-Infrared Fluorescent Proteins for Multicolor Imaging across Scales. *Nat. Commun.* **2020,** *11* (1), No. 239.

(4) Karasev, M. M.; Stepanenko, O. V.; Rumyantsev, K. A.; Turoverov, K. K.; Verkhusha, V. V. Near-Infrared Fluorescent Proteins and Their Applications. *Biochemistry (Mosc)* **2019,** *84* (Suppl 1), S32-S50.

(5) Montecinos-Franjola, F.; Lin, J. Y.; Rodriguez, E. A. Fluorescent Proteins for *in vivo* Imaging, Where's the Biliverdin? *Biochem. Soc. Trans.* **2020,** *48* (6), 2657-2667.

(6) Shcherbakova, D. M.; Baloban, M.; Emelyanov, A. V.; Brenowitz, M.; Guo, P.; Verkhusha, V. V. Bright Monomeric Near-Infrared Fluorescent Proteins as Tags and Biosensors for Multiscale Imaging. *Nat. Commun.* **2016,** *7*, No. 12405.

(7) Shcherbakova, D. M.; Baloban, M.; Pletnev, S.; Malashkevich, V. N.; Xiao, H.; Dauter, Z.; Verkhusha, V. V. Molecular Basis of Spectral Diversity in Near-Infrared Phytochrome-Based Fluorescent Proteins. *Chem. Biol.* **2015,** *22* (11), 1540-1551.

(8) Hontani, Y.; Shcherbakova, D. M.; Baloban, M.; Zhu, J.; Verkhusha, V. V.; Kennis, J. T. Bright Blue-Shifted Fluorescent Proteins with Cys in the GAF Domain Engineered from Bacterial Phytochromes: Fluorescence Mechanisms and Excited-State Dynamics. *Sci. Rep.* **2016,** *6*, No.37362.

(9) Wurth, C.; Guimard, N. K.; Hecht, M. H. Mutations that Reduce Aggregation of the Alzheimer's Aβ42 Peptide: an Unbiased Search for the Sequence Determinants of Aβ Amyloidogenesis. *J. Mol. Bio.***2002,** *319* (5), 1279-1290.

(10) Barakat, N. H.; Love, J. J. Molecular Diversity in Engineered Protein Libraries. *Curr. Opin. Chem. Biol.* **2007,** *11* (3), 335-341.

(11) Rumyantsev, K. A.; Shcherbakova, D. M.; Zakharova, N. I.; Emelyanov, A. V.; Turoverov, K. K.; Verkhusha, V. V. Minimal Domain of Bacterial Phytochrome Required for Chromophore Binding and Fluorescence. *Sci. Rep.* **2015,** *5*, No. 18348.

(12) Shcherbakova, D. M.; Verkhusha, V. V. Near-Infrared Fluorescent Proteins for Multicolor *in vivo* Imaging. *Nat. Methods* **2013,** *10* (8), 751-754.

(13) Filonov, G. S.; Piatkevich, K. D.; Ting, L. M.; Zhang, J.; Kim, K.; Verkhusha, V. V. Bright and Stable Near-Infrared Fluorescent Protein for *in vivo* Imaging. *Nat. Biotechnol.* **2011,** *29* (8), 757-761.

(14) Shcherbakova, D. M.; Baloban, M.; Verkhusha, V. V. Near-Infrared Fluorescent Proteins Engineered from Bacterial Phytochromes. *Curr. Opin. Chem. Biol.* **2015,** *27*, 52-63.

(15) Shemetov, A. A.; Oliinyk, O. S.; Verkhusha, V. V. How to Increase Brightness of Near-Infrared Fluorescent Proteins in Mammalian Cells. *Cell Chem. Biol.* **2017,** *24* (6), 758-766 e3.
(16) Campbell, B. C.; Nabel, E. M.; Murdock, M. H.; Lao-Peregrin, C.; Tsoulfas, P.; Blackmore, M. G.; Lee, F. S.; Liston, C.; Morishita, H.; Petsko, G. A. mGreenLantern: a Bright Monomeric Fluorescent Protein with Rapid Expression and Cell Filling Properties for Neuronal Imaging. *Proc. Natl. Acad. Sci. U. S. A.* **2020,** *117* (48), 30710-30721.
(17) Cranfill, P. J.; Sell, B. R.; Baird, M. A.; Allen, J. R.; Lavagnino, Z.; de Gruiter, H. M.; Kremers, G. J.; Davidson, M. W.; Ustione, A.; Piston, D. W. Quantitative Assessment of Fluorescent Proteins. *Nat. Methods* **2016,** *13* (7), 557-562.
(18) Kashiwagi, S.; Fujioka, Y.; Satoh, A. O.; Yoshida, A.; Fujioka, M.; Nepal, P.; Tsuzuki, A.; Aoki, O.; Paudel, S.; Sasajima, H.; Ohba, Y. Folding Latency of Fluorescent Proteins Affects the Mitochondrial Localization of Fusion Proteins. *Cell Struct. Funct.* **2019,** *44* (2), 183-194.
(19) Guo, Y.; Li, D.; Zhang, S.; Yang, Y.; Liu, J. J.; Wang, X; Liu, C.; Milkie, D. E.; Moore, R. P.; Tulu, U. S.; Kiehart, D. P.; Hu, J.; Lippincott-Schwartz, J.; Betzig, E.; Li, D. Visualizing Intracellular Organelle and Cytoskeletal Interactions at Nanoscale Resolution on Millisecond Timescales. *Cell* **2018,** *175* (5), 1430-1442 e17.
(20) Zhao, W; Zhao, S.; Li, L.; Huang, X.; Xing, S.; Zhang, Y.; Qiu, G.; Han, Z.; Shang, Y.; Sun, D. E.; Shan, C.; Wu, R.; Gu, L.; Zhang, S.; Chen, R.; Xiao, J.; Mo, Y.; Wang, J.; Ji, W.; Chen, X.; Ding, B.; Liu, Y.; Mao, H.; Song, B. L.; Tan, J.; Liu, J.; Li, H.; Chen, L. Sparse Deconvolution Improves the Resolution of Live-Cell Super-Resolution Fluorescence Microscopy. *Nat. Biotechnol.* **2021**. DOI: 10.1038/s41587-021-01092-2.
(21) Wall, M. A.; Coleman, D. E.; Lee, E.; Iñiguez-Lluhi, J. A.; Posner, B. A.; Gilman, A. G.; Sprang, S. R. The Structure of the G Protein Heterotrimer $G_{i\alpha1}\beta_{1\gamma2}$. *Cell* **1995,** *83*:1047-1058.
(22) Mastop, M.; Reinhard, N. R.; Zuconelli, C. R.; Terwey, F.; Gadella, T. W. J., Jr.; van Unen, J.; Adjobo-Hermans, M. J. W.; Goedhart, J. A FRET-Based Biosensor for Measuring Gα13 Activation in Single Cells. *PLoS One* **2018,** *13* (3), No. e0193705.
(23) Koelle, D. M.; Norberg, P.; Fitzgibbon, M. P.; Russell, R. M.; Greninger, A. L.; Huang, M. L.; Stensland, L.; Jing, L.; Magaret, A. S.; Diem, K.; Selke, S.; Xie, H.; Celum, C.; Lingappa, J. R.; Jerome, K. R.; Wald, A.; Johnston, C. Worldwide Circulation of HSV-2 x HSV-1 Recombinant Strains. *Sci. Rep.* **2017,** *7*, No. 44084.
(24) Pieknik, J. R.; Bertke, A. S.; Tang, S.; Krause, P. R. A VP26-mNeonGreen Capsid Fusion HSV-2 Mutant Reactivates from Viral Latency in the Guinea Pig Genital Model with Normal Kinetics. *Viruses* **2018,** *10* (5), No. 246.
(25) Morimoto, T.; Arii, J.; Tanaka, M.; Sata, T.; Akashi, H.; Yamada, M.; Nishiyama, Y.; Uema, M.; Kawaguchi, Y. Differences in the Regulatory and Functional Effects of the Us3 Protein Kinase Activities of Herpes Simplex Virus 1 and 2. *J. Virol.* **2009,** *83* (22), 11624-11634.
(26) Filonov, G. S.; Verkhusha, V. V. A Near-Infrared BiFC Reporter for *in vivo* Imaging of Protein-Protein Interactions. *Chem. Biol.* **2013,** *20* (8), 1078-1086.
(27) Tchekanda, E.; Sivanesan, D.; Michnick, S. W. An Infrared Reporter to Detect Spatiotemporal Dynamics of Protein-Protein Interactions. *Nat. Methods* **2014,** *11* (6), 641-644.
(28) Pandey, N.; Nobles, C. L.; Zechiedrich, L.; Maresso, A. W.; Silberg, J. J. Combining Random Gene Fission and Rational Gene Fusion to Discover Near-Infrared Fluorescent Protein Fragments that Report on Protein-Protein Interactions. *ACS Synth. Biol.* **2015,** *4* (5), 615-624.
(29) Chen, M.; Li, W.; Zhang, Z.; Liu, S.; Zhang, X.; Zhang, X. E.; Cui, Z. Novel Near-Infrared BiFC

Systems from a Bacterial Phytochrome for Imaging Protein Interactions and Drug Evaluation under Physiological Conditions. *Biomaterials* **2015,** *48*, 97-107.
(30) Banaszynski, L. A.; Liu, C. W.; Wandless, T. J. Characterization of the FKBP·Rapamycin·FRB Ternary Complex. *J. Am. Chem. Soc*. **2005,** *127*:4715-4721.
(31) Tiwari, D. K.; Tiwari, M.; Jin, T. Near-Infrared Fluorescent Protein and Bioluminescence-Based Probes for High-Resolution *in vivo* Optical Imaging. *Materials Advances* **2020,** *1* (5), 967-987.
(32) Rumyantsev, K. A.; Turoverov, K. K.; Verkhusha, V. V. Near-Infrared Bioluminescent Proteins for Two-Color Multimodal Imaging. *Sci. Rep.* **2016,** *6*, No. 36588.
(33) Nishihara, R.; Paulmurugan, R.; Nakajima, T.; Yamamoto, E.; Natarajan, A.; Afjei, R.; Hiruta, Y.; Iwasawa, N.; Nishiyama, S.; Citterio, D.; Sato, M.; Kim, S. B.; Suzuki, K. Highly Bright and Stable NIR-BRET with Blue-Shifted Coelenterazine Derivatives for Deep-Tissue Imaging of Molecular Events *in vivo*. *Theranostics* **2019,** *9* (9), 2646-2661.
(34) https://www.perkinelmer.com.cn/product/bioware-brite-u87mg-redfluc-bw124577.
(35) Yu, D.; Gustafson, W. C.; Han, C.; Lafaye, C.; Noirclerc-Savoye, M.; Ge, W. P.; Thayer, D. A.; Huang, H.; Kornberg, T. B.; Royant, A.; Jan, L. Y.; Jan, Y. N.; Weiss, W. A.; Shu, X.. An Improved Monomeric Infrared Fluorescent Protein for Neuronal and Tumour Brain Imaging. *Nat. Commun.* **2014,** *5*, No. 3626.
(36) Yu, D.; Baird, M. A.; Allen, J. R.; Howe, E. S.; Klassen, M. P.; Reade, A.; Makhijani, K.; Song, Y.; Liu, S.; Murthy, Z.; Zhang, S.; Weiner, O. D.; Kornberg, T. B.; Jan, Y. N.; Davidson, M. W.; Shu, X. A Naturally Monomeric Infrared Fluorescent Protein for Protein Labeling *in vivo*. *Nat. Methods* **2015,** *12* (8), 763-765.
(37) Wang, L.; Tsien, R. Y. Evolving Proteins in Mammalian Cells Using Somatic Hypermutation. *Nat. Protoc.* **2006,** *1* (3), 1346-1350.
(38) Kim, H.; Ju, J.; Lee, H. N.; Chun, H.; Seong, J. Genetically Encoded Biosensors Based on Fluorescent Proteins. *Sensors (Basel)* **2021,** *21* (3), No. 795.
(39) Massengill, C. I.; Day-Cooney, J.; Mao, T.; Zhong, H. Genetically Encoded Sensors towards Imaging cAMP and PKA Activity *in vivo*. *J. Neurosci. Methods* **2021,** *362*, No. 109298.

For TOC only